Colloid Polym Sci 273:227–232 (1995)

ORIGINAL CONTRIBUTION

C. J. G. Plummer
H.-H. Kausch

DSC non-isothermal crystallization curves in polyoxymethylene

Received: 15 April 1994
Accepted: 17 August 1994

C. J. G. Plummer (✉) · H.-H. Kausch
Laboratoire de Polymères
Ecole Polytechnique
Fédérale de Lausanne
1015 Lausanne Switzerland

Abstract Non-isothermal crystallization curves by differential scanning calorimetry for two-dimensional spherulite growth in polyoxymethylene have been modeled using the Avrami equation, taking into account heat dissipation in the sample holder during the phase transition. Good agreement is found for scanning rates up to 40 $K min^{-1}$ between experimental curves and predictions based on a knowledge of the isothermal crystallization kinetics of the same samples.

Key words Differential scanning calorimetry – polyoxymethylene – non-isothermal crystallization – Avrami equation – spherulites

Introduction

In an earlier report [1], a method was suggested for obtaining the Avrami constant $K(T)$ for heterogeneous nucleation and two-dimensional spherulitic growth in polyoxymethylene (POM) by inverting

$$X(t) = 1 - \exp\left(- \left\{ \int_0^t K(T(\tau))^{1/2} d\tau \right\}^2 \right)$$

or for constant cooling from a temperature T_0, at a constant rate α

$$X(T) = 1 - \exp\left(- \left\{ \alpha^{-1} \int_{T_0}^{T} K(\Theta)^{1/2} d\Theta \right\}^2 \right), \qquad (1)$$

where $X(T)$ is the degree of conversion at temperature T, and $K(T) = N\pi G(T)^2$, where N is the nucleation density, and $G(T)$ is the radial growth rate of the spherulites [1–4]. However, in the light of recent work [5, 6], we believe that in interpreting non-isothermal differential scanning calorimeter (DSC) curves, we did not properly take into account the heat balance between the sample pan and the furnace, leading to potentially misleading results. In what follows, the data are re-analyzed in the light of a more realistic model for the DSC response to non-isothermal crystallization [5, 6].

For the POM grades considered here, isothermal recrystallization in the range 145° to 160 °C results in spherulites of the order of 400 μm in diameter with linear interspherulite boundaries. This implies quasi-instantaneous heterogeneous nucleation. Given a constant G at a given temperature, the remaining criterion for two-dimensional Avrami behavior as described by Eq. (1) is that the samples be thin relative to the spherulite diameter. However, since doubts continue to be expressed in the literature regarding the validity of the Avrami expression, its applicability to computer simulations of two-dimensional spherulite growth under these conditions has been verified, as discussed further in Appendix I.

For practical sample sizes (~ 3 mg) the sample thickness is of the order of 70 μm, and there are deviations from Eq. (1) for short times. Thus, although acceptable fits can be obtained to isothermal DSC crystallization curves, consistent with G obtained independently by optical microscopy, and the spherulite density of the samples, it is necessary to treat the effective time delay between the start of the measurement (the time the furnace reaches the crystallization temperature) and the onset of nucleation, as an adjustable parameter [2]. This parameter is necessary to account not only for temperature lag (or overshoot), but also for transient three-dimensional spherulite growth, unless a more sophisticated analysis is undertaken. It need

Colloid & Polymer Science, Vol. 273, No. 3 (1995)

not imply the existence of a true incubation time. We have more recently used real-time image analysis of similar samples crystallized on a hot stage, which enables us to measure nucleation rates, as well as $X(t)$, and confirms that nucleation takes place on a very much shorter time scale than subsequent spherulite growth in the practically accessible temperature range (it also supports the notion that the apparent incubation time arises primarily as a result of thermal lag, and initial growth perpendicular to the plane of the sample; viewed between crossed-polarizers, relatively large nuclei appear to "loom" out of the background, rather than to appear as points) [7].

Simple image analysis also allows one to test in a crude manner for secondary crystallization behind the growth front. If the transmitted intensity is assumed to represent the local degree of crystallinity, then if there is no change in gray-level at a given point in the image within a given time interval after the passage of the growth front, it is unlikely that significant changes are occurring in the sample during this interval. This is important, since in applying Eq. (1) to samples crystallized in the DSC at constant cooling rate, apparent departures from simple Avrami behavior at high cooling rates (or equivalently, inconsistencies between two-dimensional growth and the Ozawa construction), were accounted for by secondary crystallization [1]. No corroborating evidence has been found for secondary crystallization at rates necessary to account for these effects. We now believe the explanation to be rather that at cooling rates greater than $\sim 5\,\mathrm{K\,min^{-1}}$, the analysis presented in ref. [1] is flawed. If there is a phase change, the practice of assuming the temperature of the sample to lag behind that of the furnace (the measured temperature) by some fixed amount which depends only on the cooling rate is unjustified above a certain cooling rate, and the measured signal can no longer be considered proportional to the rate of conversion, dX/dt. Fortunately, the scheme for treating non-isothermal data for polymer proposed in refs. [5, 6] allows one to take into account both the temperature differences between the sample holder and the furnace for a given heat transfer coefficient, γ, and the evolution of heat in the sample holder during the phase change. The previous analysis ignored this latter. Here, we shall only ignore temperature differences within the sample holder, which is argued to be justified for very small sample thicknesses [6].

Experimental

The samples to be discussed here were non-commercial POM homopolymer powders, containing no additives and which had undergone no thermal processing subsequent to synthesis. As received, they had a melting point of approximately 170 °C and an enthalpy of fusion of $210\,\mathrm{Jg^{-1}}$, which dropped to approximately $180\,\mathrm{Jg^{-1}}$ on recrystallization from the melt.

The measurements were carried out using the Perkin Elmer DSC 7 under nitrogen gas, with the block temperature set to 50 °C, and calibrated using indium and zinc standards. Approximately 3 mg of POM was spread uniformly on the bottom of a 10 μL aluminum pan and melted for 1 min at 200 °C prior to cooling at the desired rate. Data acquisition was carried out on an Epson Personal computer using the software provided with the DSC and the data were then transferred to a Macintosh Centris 650. All remaining computation was done using the Microsoft Excel spreadsheet and numerical analysis routines written in Pascal.

Results and discussion

During crystallization, the temperature in the DSC sample holder, T_s, obeys

$$\gamma(T_s - T_f) = -(m_s c_s + m_p c_p)\frac{dT_s}{dt} + m_s \Delta H_s \frac{dX}{dt}, \qquad (2)$$

where T_f is the furnace temperature, $\Delta H_s = 180\,\mathrm{Jg^{-1}}$ is the enthalpy of fusion per unit mass of the sample, m_s and m_p are the masses of the sample and the pan respectively, and $c_s = 2.1\,\mathrm{Jg^{-1}K^{-1}}$ and $c_p = 0.9\,\mathrm{Jg^{-1}K^{-1}}$ are their specific heats. dX/dt is assumed to be governed by Eq. (1) under equilibrium conditions, with $N = 1.9 \times 10^7\,\mathrm{m^{-2}}$ and

$$\log G(T) = 7.7 - 1.96 \times 10^5/T\Delta T - 30{,}000/2.3\,RT, \qquad (3)$$

as previously in fitting isothermal data ($\Delta T = T_0 - T$, where $T_0 = 200\,°\mathrm{C}$ is the equilibrium melting point of POM) [2]. γ was obtained from the exponential decay of the DSC heat flow curve on the high temperature side of the melting peak in a heating scan of indium as described in detail in [5], giving a value of $1.4 \times 10^{-2}\,\mathrm{WK^{-1}}$.

The heat flow rate into the sample, $\phi(T_f)$, may be predicted by setting $T_f(t) = T_0 - \alpha t$ and $T_s(0) = T_f(0) = T_0$, solving Eq. (2) numerically for $T_s(t)$ and using $\phi(T_f) = \gamma(T_s - T_f)$. Following [6], and after subtraction of the baseline, $\phi(T_f)$ may be taken to be equivalent to the measured DSC signal. Since the initial conditions are known, the calculation can be done straightforwardly using the Euler method, with recursive reduction of the time step-length Δt, to obtain stable values for $T_s(t)$. This only requires of $X(T(t))$ and its time derivative that they be calculable at $t - \Delta t$. The solid curves in Fig. 1 give predicted DSC traces for two different cooling rates.

If the term in dX/dt is ignored in calculating T_s from Eq. (2), one obtains $dT_s/dt = T_f/dt = \alpha$ and a constant

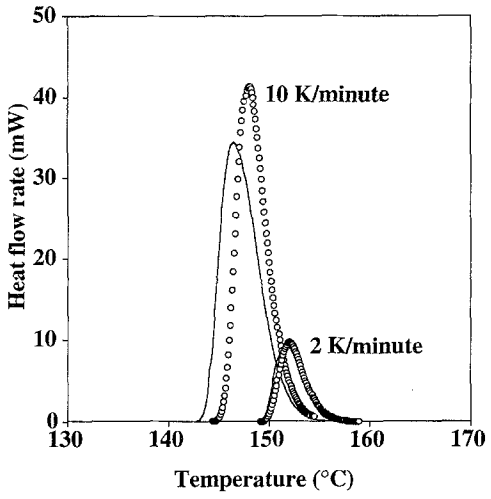

Fig. 1. Predicted DSC cooling curves for POM a) taking into account the temperature difference between the sample pan and the furnace, and b) assuming a constant temperature lag as given by Eq. (4) (open circles)

temperature lag, such that $T_s = T_f + \Delta T$, where ΔT is given by

$$\Delta T = \alpha \frac{(m_s c_s + m_p c_p)}{\gamma} . \quad (4)$$

This is the assumption generally made in treating DSC data. The difference between the measured heat flow rate and the baseline is then assumed to equal to $m_s \Delta H\, dX(T_s)/dt$ or $\alpha m_s \Delta H\, dX(T_s)/dT$, which one can calculate as a function of T_f using Eqs. (1) and (4). While this approach appears inconsistent with Eq. (2), as shown in Fig. 1, for low cooling rates, numerically determined values of $\phi(T_f)$ are very close to those calculated from $\alpha m_s \Delta H\, dX(T_s)/dT$. This is reassuring, since reasonable predictions were obtained using this latter method for $\alpha \leq 5\ \mathrm{K\,min^{-1}}$ [1]. At $\alpha = 10\ \mathrm{K\,min^{-1}}$, serious discrepancies are apparent, however, with the peak in $\phi(T_f)$ broadening, and moving to lower T_f (T_f is the temperature displayed by the DSC).

It should be noted that small errors are expected between the predictions and the data for a number of reasons. For example: heat capacities vary slightly with T; ΔH is not well characterized and may also vary within a spherulite growing non-isothermally; there will be variations in N and γ for different samples; there will be deviations from Eq. (1) at the onset of crystallization as discussed above. Further, we have no independent confirmation of the form of $G(T)$ at T less than approximately 145 °C, which represents the lower limit of the temperature range in which satisfactory isothermal measurements can be made in these samples (either optically or by DSC). Inspection of the samples suggests however that N is changing only slowly for α up to $150\ \mathrm{K\,min^{-1}}$, and that interspherulite boundaries remain linear, so that the assumption of rapid heterogeneous nucleation appears to remain valid for $T < 145$ °C.

An example of a comparison between predicted and measured values of $\phi(T_f)$ is given in Fig. 2 for various α, and a POM sample of $M_w \sim 36{,}000\ \mathrm{g\,mol^{-1}}$, showing reasonable agreement up to $\alpha = 40\ \mathrm{K\,min^{-1}}$. One might therefore infer from this that the expression for $G(T)$ in Eq. (3) remains useful for T below 145 °C. One must be careful however since (a) $T_s > T_f$ and (b) since the form of the curves at temperatures below the peak become dominated by the heat transfer coefficient and dX/dt falls to zero (the DSC trace reflects the decay of the sample temperature back to that anticipated in the absence of a phase change once the phase change is substantially complete). In fact, the sample temperature corresponding to the peak in the predicted and measured curves at $\alpha = 40\ \mathrm{K\,min^{-1}}$ is approximately 145 °C, so that while the present analysis resolves the discrepancy between the isothermal and non-isothermal measurements for cooling rates in the range 5 to $40\ \mathrm{K\,min^{-1}}$, it does not tell us anything new about $K(T)$. That the predictive power of the model breaks down at higher α is not surprising, since the DSC is not designed to operate at such cooling rates. Certainly, at $\alpha = 100\ \mathrm{K\,min^{-1}}$, the observed crystallization peak has moved to a value of T_f some 10 K below that expected. We note however that the form of the low temperature part of the curve suggests that this is not as a result of changes in γ, and indeed that the overall form of the curve is similar to that of the model curve, but simply shifted to lower T.

Fig. 2. Comparison of predicted (solid lines) and experimental DSC cooling curves for POM, $M_w \sim 36\,000\ \mathrm{g\,mol^{-1}}$

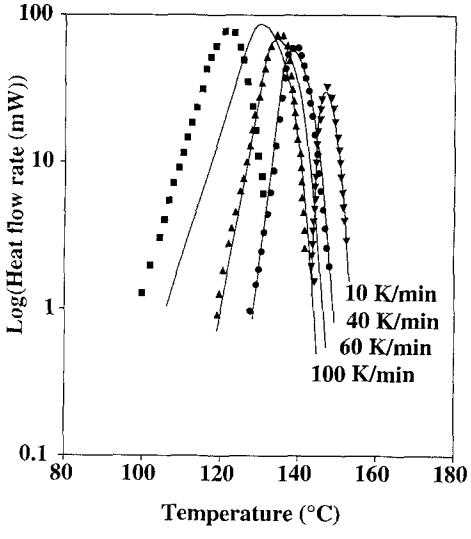

Colloid & Polymer Science, Vol. 273, No. 3 (1995)

Indeed, by adding a constant to the furnace temperature T_f, good fits can be obtained at scanning rates up to 150 K min^{-1}, which suggests the sample behavior has not altered radically. Certainly the relatively flat baselines observed at high α indicate that if there is a difference between the furnace temperature and the displayed temperature, then it will be constant.

One may also reverse the analysis to reconstruct conversion rates as a function of time from the data, and these can in principal be analyzed by inverting Eq. (1) as discussed in ref. [1]. T_s and dT_s/dt may be estimated using

$$T_s = \frac{\phi(T_f)}{\gamma} + T_f + \alpha\frac{(m_s c_s + m_p c_p)}{\gamma},$$

and

$$\frac{dT_s}{dt} = \frac{1}{\alpha}\left(1 + \frac{d\phi(T_f)}{\gamma dT_f}\right), \quad (5)$$

and dX/dt can then be obtained from Eq. (2). The numerical differentiation is very sensitive to the choice of γ, particularly in the low T region of the peak where dX/dt is approaching zero. However, one may adjust γ so that dX/dt is well behaved at low T, which is equivalent to determining it directly from each DSC run. This is in any case probably better practice than using the value taken from the indium standard, since sample pans are never identical (in spite of this, γ is found to vary only by about 10% between runs). Finally, since ΔH is not known with any great certainty, dX/dt is integrated with respect to time in order to check that the final value of X is close to unity, and adjust ΔH if necessary. At high cooling rates, ΔH diminished somewhat, but was never more than 10% less than the value of 180 J g^{-1} assumed above. Examples of apparent and corrected dX/dt are given in Fig. 3 as a function of the temperature reading on the DSC (which should be considered here as an indication of the evolution of time rather than temperature, particularly in view of the comments made regarding the possibility of lag in T_f itself).

Fig. 3. dX/dt as a function of the nominal temperature displayed by the DSC calculated assuming constant dT_s/dt (open squares) and dX/dt corrected for variations in dT_s/dt (filled squares)

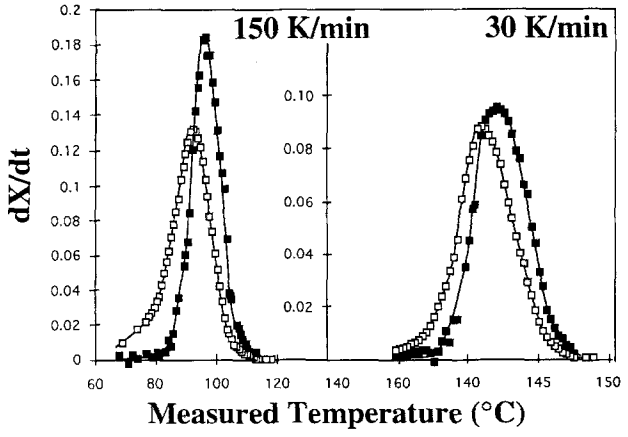

Conclusion

It is unfortunately difficult at present to analyse curves such as those in Fig. 3 using Eq. (1), since this involves a further numerical differentiation step. Figure 4 shows the current results, including data for $\alpha > 40$ K min^{-1} which have been shifted to higher temperatures. The results are expressed as $K(T_s)$ against T_s to facilitate comparison with the results of ref. [1]. In spite of the crudeness of the analysis, we feel that the secondary crystallization model in its original form may be dismissed, although the problem remains of whether one can assume a constant temperature lag between T_f and the displayed temperature at cooling rates of 60 K min^{-1} and above. This is not only of technological interest (for injection molding or other forming processes involving high cooling rates), but also of fundamental interest in that entanglement constraints in the melt will begin to influence the relaxation of crystallizing chains very strongly in precisely this temperature regime, and so we might anticipate changes in the transport phenomena contributing to G(T) [8]. Unfortunately, it is not possible to say at this stage whether the apparent downturn in $K(T_s)$ obtained at $\alpha > 150$ K min^{-1} is indicative of this. On a more general note, this work serves to underline the dangers pointed out in refs. [5, 6] of too

Fig. 4. $K(T)$ values estimated using Eq. (1) and corrected data. The solid line was derived independently from optical measurements. The filled symbols are results for $\alpha = 100$ and 150 Kmin^{-1} prior to shifting along the T axis

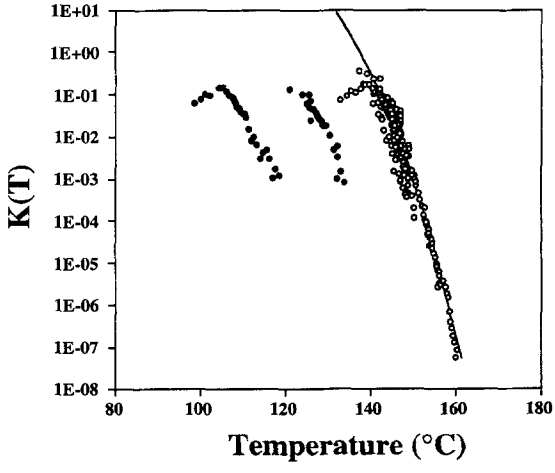

naive an interpretation of non-isothermal DSC data of polymers at high cooling rates.

Appendix I

The computer simulation of spherulite growth for two-dimensional growth at constant G and instantaneous nucleation at a fixed number of randomly distributed sites is easily implemented. In this case, NA in a typical DSC sample is about 200 (A is the sample area). White spherulites were allowed to grow on a black computer screen with a radial velocity of 4 pixels per unit time (unit time corresponding to the execution of growth step in the program), and the total number of white pixels was determined within a box of dimensions 200×300 pixels containing NA spherulites, as shown in Fig. A1 (out of a total of $2NA$). Figure A2 shows the measured behavior and the behavior predicted by the Avrami equation for $NA \sim 25$, 50, and 500.

Fig. A1. Computer simulated final spherulitic textures for two-dimensional growth with instantaneous heterogeneous nucleation, where the total number of spherulites is 100, 200, and 2000, as indicated (the "Maltese crosses" are omitted when calculating X), and the computed X values are taken from the central rectangular region (containing approximately 25,50, and 500 spherulites in the respective cases)

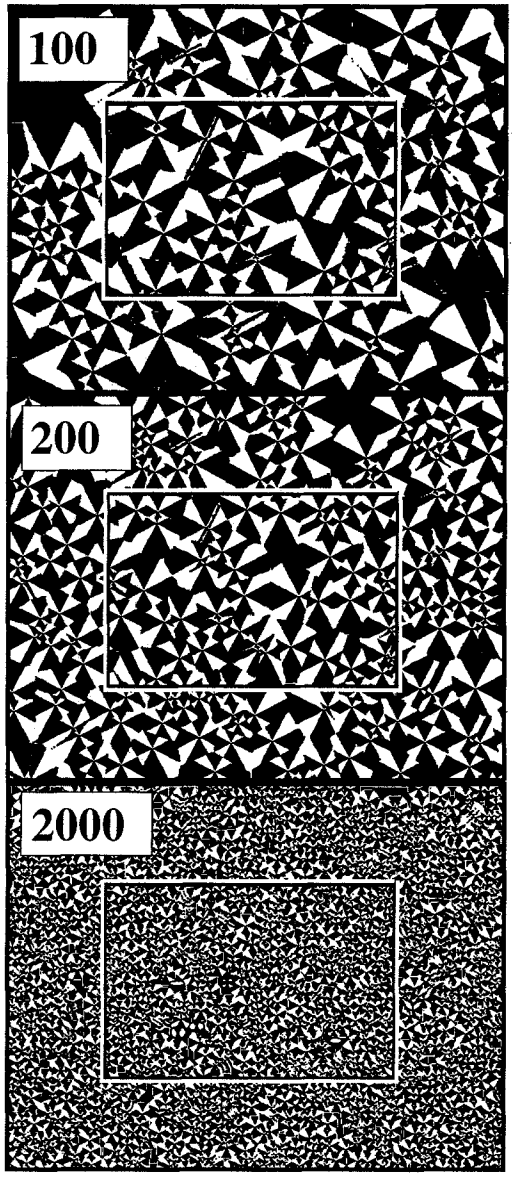

It was recently suggested that the behavior of POM might be better described by using expressions derived from the Tobin model [9] as an *alternative* to the Avrami expression [10]. In view of Fig. A2, this seems unlikely in the present case. The Tobin model involves calculating the spherulite sizes at time t, and then calculating the total area covered when a certain number of spherulites is placed at random positions within a confined region. In two-dimensions, for a nucleation density N, this is equivalent to adding NA discs of area δA to a surface of area A, where for instantaneous nucleation $\delta A = \pi(Gt)^2$. After addition of the first spherulite, the area fraction of crystalline material is

$$X_1 = \frac{\delta A}{A} .$$

After addition of the second spherulite, since its position can be anywhere within the box, the expectation of X is

$$X_2 = \frac{\delta A}{A} + \frac{\delta A}{A}\left(1 - \frac{\delta A}{A}\right) = 2\frac{\delta A}{A} - \left(\frac{\delta A}{A}\right)^2 ,$$

Fig. A2. Comparison of the evolution of X in the simulations of Fig. A1 and the values predicted by the Avrami expression (solid lines)

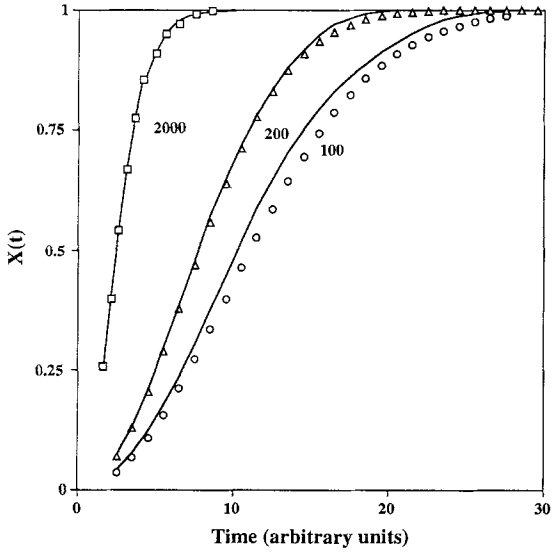

since, averaged over a large number of trials, one would find that a fraction $1 - X_1$ of the area of the second spherulite will be occluded by the first. Similarly,

$$X_3 = 2\frac{\delta A}{A} - \left(\frac{\delta A}{A}\right)^2 + \frac{\delta A}{A}\left(1 - 2\frac{\delta A}{A} + \left(\frac{\delta A}{A}\right)^2\right)$$
$$= 3\frac{\delta A}{A} - 3\left(\frac{\delta A}{A}\right)^2 + \left(\frac{\delta A}{A}\right)^3,$$

and so on. In other words, $1 - X_{NA}$ obeys a binomial distribution with mean $\mu = NA.\delta A/A = N\pi(Gt)^2$, or in the limit of large NA and small $\delta A/A$,

$$X = 1 - \exp(-N\pi(Gt)^2$$

Thus, for two-dimensional growth with instantaneous heterogeneous nucleation, the Tobin model simply reverts to the Avrami expression with $n = 2$.

Acknowledgement The financial support of DuPont de Nemours Ltd. is gratefully acknowledged.

References

1. Plummer CJG, Kausch H-H (1994) J Mat Sci Lett 13:856
2. Plummer CJG, Kausch H-H (1994) Polym Bull 32:117
3. Ozawa T (1970) Polymer 12:150
4. Cao (1992) J Polym Commun 33:3520
5. Janeschitz-Kriegl H, Wippel H, Paulik C, Eder G (1993) Colloid Polym Sci 271:1107
6. Wu CH, Eder G, Janeschitz-Kriegl H (1993) Colloid Polym Sci 271:1116
7. Plummer CJG, Kausch H-H (1994) Unpublished results, Lausanne
8. Plummer CJG, Menu P, Cudré-Mauroux N, Kausch H-H, Submitted to J Appl Poly Sci
9. Tobin MC (1974) J Poly Sci, Poly Phys Ed. 12:399
10. Cruz-Pinto JJC, Martins JA, Oliviera MJ (1994) Colloid Polym Sci 272:1